P Selected for a Viewpoint in *Physics*

ℰ

Kaleidoscope of Exotic Quantum Phases in a Frustrated *XY* Model

Christopher N. Varney,[1,2] Kai Sun,[1,3] Victor Galitski,[1,3] and Marcos Rigol[2]

[1]*Joint Quantum Institute and Department of Physics, University of Maryland, College Park, Maryland 20742, USA*
[2]*Department of Physics, Georgetown University, Washington, D.C. 20057, USA*
[3]*Condensed Matter Theory Center, Department of Physics, University of Maryland, College Park, Maryland 20742, USA*

The existence of quantum spin liquids was first conjectured by Pomeranchuk some 70 years ago, who argued that frustration in simple antiferromagnetic theories could result in a Fermi-liquid-like state for spinon excitations. Here we show that a simple quantum spin model on a honeycomb lattice hosts the long sought for Bose metal with a clearly identifiable Bose surface. The complete phase diagram of the model is determined via exact diagonalization and is shown to include four distinct phases separated by three quantum phase transitions.

We learn early in our education that as matter is cooled down to low temperatures it normally experiences transitions into ordered states of various kinds—crystalline solid structures, ordered magnetic phases, superfluid and superconducting states, etc. It is also common knowledge that upon heating the matter, the ordered phases melt into the familiar gaseous or liquid classical states that we encounter routinely in our everyday lives. A more specialized but equally well-established result is that no order that breaks a continuous symmetry can survive in one-dimensional systems [1], because quantum zero-point motion acts there similarly to thermal effects and "quantum-melts" ordered phases even at zero temperature.

It has been a long-standing and important question in physics whether quantum fluctuations in higher-dimensional quantum spin or boson systems can have the same debilitating effect, giving way to quantum liquids [2]. The interest in such a hypothetical spin liquid, also known as a Bose or spin metal [3], has experienced multiple revivals with the most prominent one associated with the discovery of high-temperature superconductivity [4,5]. However, despite the decades of intensive search, no convincing examples of a gapless spin liquid have been found in any realistic two-dimensional quantum model.

In models that are fermionizable via the Jordan-Wigner transformation [6,7], the existence of spin liquids has now been firmly established [7,8], but the physics there mimics somewhat the one-dimensional result [9–11]. What remains of crucial importance is whether a truly higher-dimensional spin system may host a quantum liquid. Among the influential recent results here are the stability argument by Hermele *et al.* [12], who showed that there is no fundamental obstacle to the existence of quantum spin liquids, and a complete classification of quantum orders by Wen [13], who demonstrated that an amazing variety of hypothetical gapless spin liquids can all be divided into several distinct classes, which include stable phases with

low-lying fermionic spinon excitations that resemble a Fermi-liquid state. Also, the work of Motrunich, Fisher, and Sheng [14,15] provides strong arguments in favor of the existence of such putative two-dimensional Bose metals and suggests that the strong singularity in the spin structure factor at a Bose surface is one of the hallmark phenomena of this exotic state.

The main idea is that, despite the fact that the underlying particles are bosons, the collective behaviors in these strongly correlated Bose-metal states show a strong analogy to a Fermi liquid formed by fermionic particles. In a Fermi liquid, the fermion statistics dictate the formation of Fermi surfaces, which possess singular behavior. In a Bose metal, despite the absence of Pauli's principle, similar singularities also arise and define a surface in momentum space, known as a Bose surface [14,15]. The existence of a Bose surface is the key property and most striking experimental feature of a Bose metal. However, unlike a Fermi liquid, where the Luttinger theorem requires that the Fermi wave vector depends on the density of fermions, the Bose wave vector in a Bose metal depends on the control parameters and can vary continuously even at fixed particle density.

Here we provide strong evidence that a model as simple as the *XY*-spin model on a honeycomb lattice with nearest-neighbor (NN) and next-to-nearest-neighbor (NNN) interactions hosts, among other phases, a Bose metal with a clearly identifiable Bose surface. Although we came across this finding serendipitously, we would like to provide qualitative arguments that could potentially guide searches for other such interesting spin models. Note that the description of a spin Fermi-liquid-like state is necessarily a gauge theory [5,16,17], which is very similar to that of the Halperin-Lee-Read [18] quantized Hall (QH) state. In the latter gapless phase, the interacting electron system in a large classical external field gives rise to composite fermions in zero classical field but coupled to a fluctuating

quantum field—the Chern-Simons field that implements flux attachment. The natural question here, considered before, e.g., in Refs. [19,20], is whether a fractional QH state of this or any other type is possible in a sensible lattice model.

The above remarks are relevant to our work because our simple Hamiltonian, see Eq. (1) below, can be viewed as a natural "trial model" for such a possible fractional lattice QH state per the following construction. Take the Haldane model [21] of noninteracting electrons on a honeycomb lattice with simple NN hoppings and complex NNN hoppings, $|J_2|e^{i\phi}$. If ϕ is nonzero it realizes a topological insulator or lattice "integer" QH state. Replace the fermions with hard-core bosons at half-filling [22] and it becomes a promising strongly interacting model. Notably, the most frustrated limit corresponds to $\phi = \pi$, which maps at half-filling to the following Hamiltonian

$$H = J_1 \sum_{\langle ij \rangle} (b_i^\dagger b_j + \text{H.c.}) + J_2 \sum_{\langle\langle ij \rangle\rangle} (b_i^\dagger b_j + \text{H.c.}), \quad (1)$$

where $b_i^\dagger$ (b_i) is an operator that creates (annihilates) a hard-core boson on site i. Here, we require the sign of J_2 to be positive (that is, $\phi = \pi$), while the sign of J_1 is in fact irrelevant because of the particle-hole symmetry of the honeycomb lattice ($b_i \rightarrow -b_i$ for one of the two sublattices). In what follows, $J_1 = 1$ sets our unit of energy. Note that Hamiltonian (1) maps to a frustrated antiferromagnetic-XY model ($b_i^\dagger \rightarrow S_i^+$ and $b_i \rightarrow S_i^-$),

$$H = J_1 \sum_{\langle ij \rangle} (S_i^+ S_j^- + \text{H.c.}) + J_2 \sum_{\langle\langle ij \rangle\rangle} (S_i^+ S_j^- + \text{H.c.}). \quad (2)$$

The properties of this Hamiltonian are governed by the dimensionless control parameter J_2/J_1. The limits of this model are well understood. For $J_2/J_1 = 0$, the ground state of this Hamiltonian is an antiferromagnet [Fig. 1(b)]. When $J_2/J_1 \rightarrow \infty$, however, the ground state is a spin wave with 120° order [Fig. 1(d)]. Because the system is highly frustrated, there is a strong possibility of intermediate phases. In Fig. 1(a), we show the phase diagram for 24-site clusters as a function of J_2/J_1, finding two intermediate phases: (1) a quantum spin liquid and (2) an exotic spin wave state [Fig. 1(c)].

To pin down the phase boundaries, we consider the ground-state fidelity metric g, which has been shown to be an unbiased and sensitive indicator of quantum phase transitions [23,24]. In Fig. 2(a), we show the fidelity metric for three different 24-site clusters [22,25]. There are three peaks in g, indicating three quantum phase transitions. As we discuss in greater detail below, the three clusters have slightly different momentum space representations, resulting in the second and third transitions to occur at slightly different values of J_2/J_1 for each cluster.

Another indicator of a phase transition can be seen in the NN energy E_1 (the NNN energy is denoted by E_2). In Fig. 2(b), we show the ratio E_1/E (here E is the ground-state energy) for the 24D cluster. The transition points are directly connected with the inflection points in E_1/E. To demonstrate this more clearly, we also show the derivative of E_1/E, whose minima coincide with the transitions determined by the fidelity metric.

From the mapping between spins and hard-core bosons, it follows that the antiferromagnetic and the other two ordered states correspond to Bose-Einstein condensates (BECs) in which bosons condense into quantum states with different momenta. To characterize these phases, we measure the condensate fraction $f_c = \Lambda_1/N_b$ (N_b is the total number of bosons) by computing the largest eigenvalue Λ_1 of the one-particle density matrix $\rho_{ij} = \langle b_i^\dagger b_j \rangle$. If f_c scales to a nonzero value in the thermodynamic limit, then the system exhibits Bose-Einstein condensation [26]. This is the case in three of our phases, as depicted in
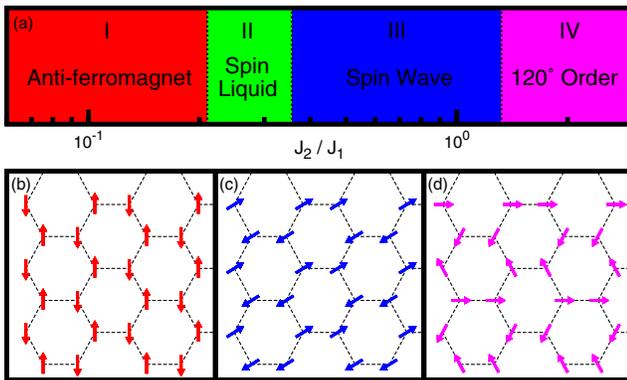
FIG. 1 (color online).   (a) Phase diagram of the model in Eq. (1) as a function of J_2/J_1, (b) antiferromagnetic ordering (phase I), (c) spin wave ordering with wave vector $\mathbf{k} = M$ (phase III), (d) collinear spin wave ordering with wave vector $\mathbf{k} = K$ (phase IV). The phase boundaries are $(J_2/J_1)_{\text{I}\rightarrow\text{II}} = 0.210 \pm 0.008$, $(J_2/J_1)_{\text{II}\rightarrow\text{III}} = 0.356 \pm 0.009$, and $(J_2/J_1)_{\text{III}\rightarrow\text{IV}} = 1.320 \pm 0.020$.
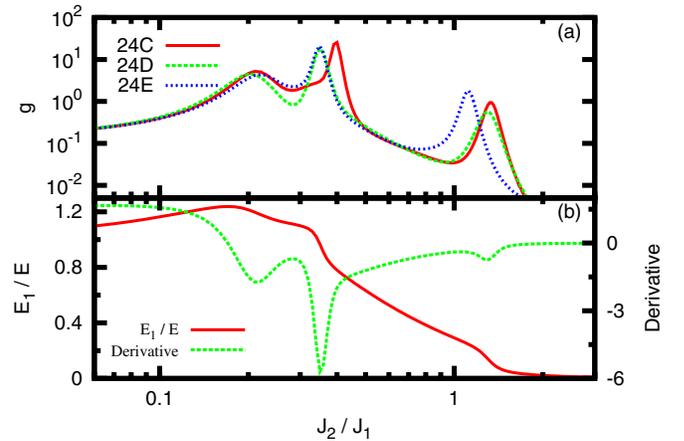
FIG. 2 (color online).   (a) Fidelity metric vs J_2/J_1 for clusters 24C, 24D, and 24E. (b) Ratio of the NN energy to the total energy E_1/E and its derivative (right axis) for the 24D cluster.
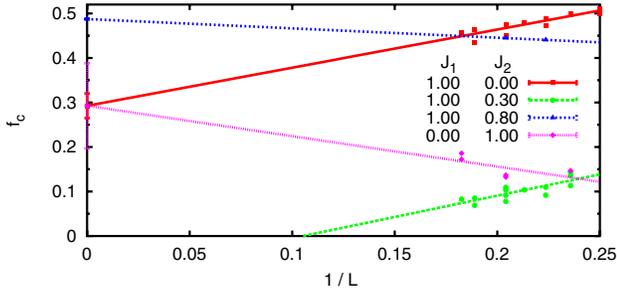
FIG. 3 (color online). Finite-size scaling of the condensate fraction f_c for parameters that are representative of each phase depicted in Fig. 1 ($J_2/J_1 = 0.00, 0.30, 0.80, \infty$). The color of each curve is consistent with the color coding in Fig. 1. In the limit $L \to \infty$, the condensate fraction is nonzero in the antiferromagnetic, spin wave, and 120° ordered phases.

Fig. 3. For the Bose-metal phase, on the other hand, the condensate fraction vanishes in the thermodynamic limit, indicating the absence of BEC.

To further examine the properties of these phases, we calculate the single-particle occupation at different momentum points

$$n(\mathbf{k}) = \langle \alpha_{\mathbf{k}}^{\dagger} \alpha_{\mathbf{k}} \rangle + \langle \beta_{\mathbf{k}}^{\dagger} \beta_{\mathbf{k}} \rangle. \qquad (3)$$

Here, $\alpha_{\mathbf{k}}$ and $\beta_{\mathbf{k}}$ are boson annihilation operators at momentum $\mathbf{k}$ for the A and B sublattices. Because we are studying finite-sized clusters, we utilize twisted boundary conditions [27] and average over 40×40 boundary conditions to fully probe the Brillouin zone.

In Fig. 4, we show the momentum distribution function as a function of $\mathbf{k}$ for select values of J_2/J_1 that are representative of each phase. In the first phase [Fig. 4(a)], the momentum distribution function is sharply peaked at $\mathbf{k} = \Gamma$, indicating an antiferromagnetically ordered
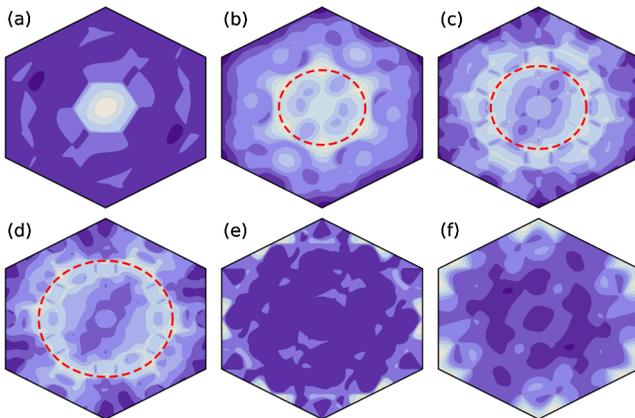
FIG. 4 (color online). $n(\mathbf{k})$ vs $\mathbf{k}$ for (a) the Néel state ($J_2/J_1 = 0$), (b)–(d) Bose metal ($J_2/J_1 = 0.27, 0.30,$ and 0.32), (e) collinear spin wave ($J_2/J_1 = 0.80$), and (f) the 120° ordered state ($J_2/J_1 = \infty$). In (b)–(d), the Bose surface is indicated by the dashed red line and has a radius of magnitude $k_B = 0.9, 1.0,$ and 1.4, respectively. Each plot contains 19 600 k points.

state. The third and fourth phases [Figs. 4(e) and 4(f), respectively] also exhibit sharp peaks in $n(\mathbf{k})$, but this time at the edges of the Brillouin zone. For phase III [Fig. 4(e)], $n(\mathbf{k})$ is maximal at $\mathbf{k} = M$, corresponding to the collinear spin wave state illustrated in Fig. 1(c). For phase IV [Fig. 4(f)], $n(\mathbf{k})$ is maximal at $\mathbf{k} = K$, as one would expect for a 120° ordered phase [Fig. 1(d)].

The momentum distribution function in the Bose metal is depicted in Figs. 4(b)–4(d) for three different values of J_2/J_1. One can see there that $n(\mathbf{k})$ in this phase exhibits a remarkable J_2/J_1-dependent Bose surface. Namely, the magnitude of the Bose wave vector k_B at which the maxima of $n(\mathbf{k})$ occurs changes (increases) with increasing J_2/J_1. The important distinction to be made here is that those maxima do not reflect Bose-Einstein condensation; i.e., they do not scale with the system size as the ones in the other three phases do.

We should add that, in order to exclude other ordering tendencies in phase II, we also examined the S^z correlation function $C_{i,j} = \langle (S_{ia}^z - S_{ib}^z)(S_{ja}^z - S_{jb}^z) \rangle$ and the dimer-dimer correlation function $D_{ij,k\ell} = \langle (\mathbf{S}_i \cdot \mathbf{S}_j)(\mathbf{S}_k \cdot \mathbf{S}_\ell) \rangle$ and their corresponding structure factors. Finite-size scaling of these structure factors (not shown) made evident that neither charge density wave formation nor dimer formation occurs. We also computed the excitation gap in the Bose-metal phase and found it to be much smaller than the (finite-size) excitation gap in the antiferromagnetic state. In the antiferromagnetic phase, the system is gapless in the thermodynamic limit, due to the spontaneous breaking of the spin-rotation symmetry and the resulting Goldstone modes. Since the gap in the Bose-metal phase is significantly smaller, we believe this gap is also due to finite-size effects and will close in thermodynamic limit. Our small system sizes prevent us from reaching conclusive results for this quantity after a finite-size extrapolation. Nevertheless, all the phenomena we observed in this phase are consistent with and indicate a Bose-metal phase.

In Fig. 5, we illustrate how both the momentum distribution function and the largest eigenvalue of $\langle \alpha_i^{\dagger} \alpha_j + \beta_i^{\dagger} \beta_j \rangle$, λ_1, evolve over the entire parameter space for two different 24-site clusters with periodic boundary conditions. The maximum of $n(\mathbf{k})$ perfectly matches λ_1, and it is clear that the momenta of the condensates in phases I, III, and IV are $\mathbf{k} = \Gamma$, M, and K, respectively. In addition, it can be seen that the momentum distribution in phase II exhibits a peak inside the Brillouin zone that shifts to larger momenta as J_2/J_1 is increased.

Phases III and IV exhibit an interesting phenomenon that can be unveiled by examining the degeneracy of the largest eigenvalues of the one-particle density matrix. In an ordinary BEC state, condensation occurs to a unique effective single-particle state, and thus the largest eigenvalue of the density matrix is nondegenerate and $O(N_b)$, while the second largest eigenvalue is already $O(1)$. This is what we find in the antiferromagnetic state (phase I). However,
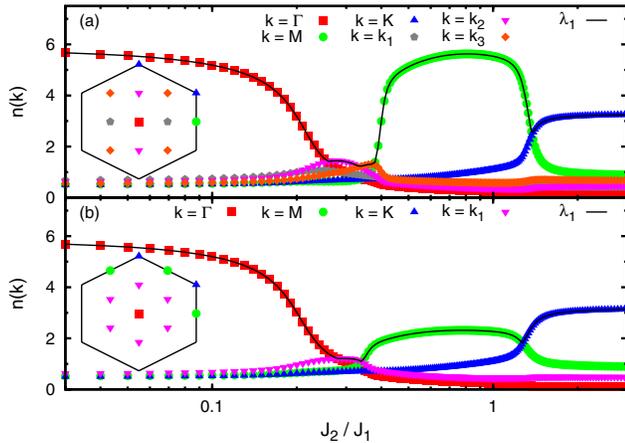
FIG. 5 (color online). Momentum distribution function (symbols) for the different values of **k** and clusters (a) $24C$ and (b) $24D$. Also shown are the largest eigenvalue λ_1 of the single-particle density matrix (line). The inset of each panel illustrates the k points for each cluster.

in general, condensation can occur to more than one effective one-particle state [28,29], and various largest eigenvalues of the one-particle density matrix may become $O(N_b)$ and degenerate. This fragmentation occurs in phases III and IV. For phase IV, it is trivial to realize that the condensate must be degenerate in the limit $J_2/J_1 \rightarrow \infty$, where the system consists of two disconnected triangular lattices. Interestingly, in this model, fragmentation occurs for all values of J_2/J_1 in phases III and IV, and is related to the number of M or K points present in the clusters under consideration.

In summary, we have studied a frustrated XY model on a honeycomb lattice. We find that this model exhibits four phases [see phase diagram in Fig. 1(a)]: (I) a BEC at $\mathbf{k} = \Gamma$ (antiferromagnetism), (II) a Bose metal (spin liquid), (III) a BEC at $\mathbf{k} = M$ (a collinear spin wave), and (IV) a BEC at $\mathbf{k} = K$ (120° order). The Bose-metal phase is characterized by a parameter dependent peak in $n(\mathbf{k})$ and a lack of condensation, solid order, and dimer order. This work provides the first convincing example of a gapless spin liquid in a surprisingly simple model of XY spins. We believe that there is no fundamental challenge to realize the Bose-metal phase in experimental systems dealing with spins or ultracold optically trapped bosons in the regime of large on-site Hubbard repulsion. Finally, recent experimental [30] and theoretical [31–34] work suggest that exotic quantum spin liquids might exist in related lattice models for $SU(2)$ spins. It would be interesting to see what relationship, if any, exists between these possible $SU(2)$ spin liquids and our Bose metal, which can be studied by introducing interaction terms for the bosons.

[1] M. A. Cazalilla *et al.*, arXiv:1101.5337 [Rev. Mod. Phys. (to be published)].
[2] I. Y. Pomeranchuk, Zh. Eksp. Teor. Fiz. **11**, 226 (1941).
[3] Note that since spin-1/2 models can be mapped onto hard-core boson models and vice versa, one can use the terms "spin liquid" and "Bose liquid" (also "Bose metal") interchangeably when referring to such states.
[4] P. W. Anderson, Science **235**, 1196 (1987).
[5] P. A. Lee, N. Nagaosa, and X.-G. Wen, Rev. Mod. Phys. **78**, 17 (2006).
[6] P. Jordan and E. Wigner, Z. Phys. A **47**, 631 (1928).
[7] V. Galitski, Phys. Rev. B **82**, 060411(R) (2010).
[8] A. Paramekanti, L. Balents, and M. P. A. Fisher, Phys. Rev. B **66**, 054526 (2002).
[9] V. J. Emery *et al.*, Phys. Rev. Lett. **85**, 2160 (2000).
[10] A. Vishwanath and D. Carpentier, Phys. Rev. Lett. **86**, 676 (2001).
[11] R. Mukhopadhyay, C. L. Kane, and T. C. Lubensky, Phys. Rev. B **64**, 045120 (2001).
[12] M. Hermele *et al.*, Phys. Rev. B **70**, 214437 (2004).
[13] X.-G. Wen, Phys. Rev. B **65**, 165113 (2002).
[14] O. I. Motrunich and M. P. A. Fisher, Phys. Rev. B **75**, 235116 (2007).
[15] D. N. Sheng, O. I. Motrunich, and M. P. A. Fisher, Phys. Rev. B **79**, 205112 (2009).
[16] L. B. Ioffe and A. I. Larkin, Phys. Rev. B **39**, 8988 (1989).
[17] O. I. Motrunich, Phys. Rev. B **72**, 045105 (2005).
[18] B. I. Halperin, P. A. Lee, and N. Read, Phys. Rev. B **47**, 7312 (1993).
[19] A. Seidel *et al.*, Phys. Rev. Lett. **95**, 266405 (2005).
[20] A. A. Burkov, Phys. Rev. B **81**, 125111 (2010).
[21] F. D. M. Haldane, Phys. Rev. Lett. **61**, 2015 (1988).
[22] C. N. Varney *et al.*, Phys. Rev. B **82**, 115125 (2010).
[23] P. Zanardi and N. Paunkovi, Phys. Rev. E **74**, 031123 (2006).
[24] M. Rigol, B. S. Shastry, and S. Haas, Phys. Rev. B **80**, 094529 (2009).
[25] See Supplemental Material at http://link.aps.org/supplemental/10.1103/PhysRevLett.107.077201 for a description of the ground-state fidelity and the clusters used in this study.
[26] O. Penrose and L. Onsager, Phys. Rev. **104**, 576 (1956).
[27] D. Poilblanc, Phys. Rev. B **44**, 9562 (1991).
[28] A. J. Leggett, Rev. Mod. Phys. **73**, 307 (2001).
[29] T. D. Stanescu, B. Anderson, and V. Galitski, Phys. Rev. A **78**, 023616 (2008).
[30] Y. J. Yan *et al.*, arXiv:1106.1713.
[31] Z. Y. Meng *et al.*, Nature (London) **464**, 847 (2010).
[32] A. Mulder *et al.*, Phys. Rev. B **81**, 214419 (2010).
[33] B. K. Clark, D. A. Abanin, and S. L. Sondhi, arXiv:1010.3011.
[34] A. F. Albuquerque *et al.*, Phys. Rev. B **84**, 024406 (2011).